International Journal of High Throughput Screening

Dovepress
open access to scientific and medical research

Open Access Full Text Article

ORIGINAL RESEARCH

The development of a high-throughput/combinatorial workflow for the study of porous polymer networks

This article was published in the following Dove Press journal:
International Journal of High Throughput Screening
5 April 2012
Number of times this article has been viewed

Partha Majumdar[1]
James Bahr[1]
Elizabeth Crowley[1]
Alekhya Kallam[1]
Nathan Gubbins[1]
Kris Schiele[1]
Michael Weisz[1]
Shawn M Dirk[2]
Joseph L Lenhart[3]
Bret J Chisholm[1,4]

[1]Center for Nanoscale Science and Engineering, [2]Sandia National Laboratories, Albuquerque, New Mexico, [3]US Army Research Laboratory, Aberdeen, Maryland, [4]Department of Coatings and Polymeric Materials, North Dakota State University, Fargo, North Dakota, USA

Abstract: A high-throughput workflow was developed for the study of porous polymers generated using the process of chemically induced phase separation. The workflow includes automated, parallel preparation of liquid blends containing reactive, polymer network-forming precursors and a poragen, as well as a high-throughput poragen extraction process using supercritical CO_2. A structure–process–property relationship study was conducted using epoxy-amine cross-linked networks. The experimental design involved variations in polymer network cross-link density, poragen composition, poragen level, and cure temperature. A total of 216 unique compositions were prepared. Changes in opacity of the blends as they cured were monitored visually. Morphology was characterized using a scanning electron microscope on a subset of the 216 samples. The results obtained allowed for the identification of compositional variables and process variables that enabled the production of porous networks.

Keywords: high-throughput, chemically induced phase separation, porous polymer, poragen

Introduction

Porous polymer materials are of interest for a wide variety of applications such as tissue scaffolds,[1] controlled drug release,[2] chromatography,[3] separation membranes,[4] piezoelectric materials,[5] chemical sensors,[6,7] hydrogen storage materials,[8,9] and battery electrodes.[10] Several general methods for creating porous polymers have been described. These methods include conventional foaming techniques involving a nonreactive gas,[11] emulsion-templating,[12,13] thermally induced phase separation,[14] chemically induced phase separation (CIPS),[15] selective degradation of block copolymers,[16] and molecular imprinting.[17] Relative to the other methods for producing porous polymer materials, CIPS probably provides the greatest versatility with respect to the range of materials that can be generated. In addition, the process to produce porous materials using CIPS is relatively straightforward and a large number of readily available starting materials can be utilized.

The process for producing porous polymer materials using CIPS involves the cross-linking of a homogeneous blend comprised of reactive precursors and a nonreactive component referred to as a poragen.[15,18,19] Due to the increase in the free energy of mixing that occurs as reaction takes place between the reactive precursors, the poragen phase separates from the mixture during the process of cross-linking. Porosity is generated by removal of the poragen from the cross-linked material using an extraction or evaporation process. The pore size, pore shape, and pore size distribution obtained with this process is a result of the complex interaction between the thermodynamics

Correspondence: Bret Chisholm
Center for Nanoscale Science and Engineering, North Dakota State University, 1805 Research Park Drive, Fargo, ND 58102, USA
Tel +1 701 231 5328
Fax +1 701 231 5325
Email bret.chisholm@ndsu.edu

of mixing, kinetics of cross-linking, and kinetics of phase separation. Figure 1A displays a schematic of the process used to prepare a porous network structure using CIPS.

With CIPS, a stable solution is transformed into a phase-separated material without a change in temperature. Phase separation in CIPS is the result of the decrease in entropy created by the increase in polymer molecular weight that occurs as a result of cross-linking reactions. Kiefer and coworkers[15] modified the Flory–Huggins equation so that it can be applied to reactive solutions. The modified equation is $\Delta G^V = (\Delta G/V_T) = RT/V_0 \{(1–4/3q)\ \phi_{pol} \ln \phi_{pol} + (\phi_{sol}/Z_{sol}) \ln \phi_{sol}\} + |\vec{d}\ (q)|^2\ \phi_{pol}\ \phi_{sol}$, where ΔG^V is the change in free energy of the system per unit volume, ΔG is the change in free energy of the system, V_T is the total free volume, R is the gas constant, T is temperature, V_0 is the molar volume of precursor monomers, q is the extent of reaction or conversion, ϕ_{pol} is the volume fraction of polymer, ϕ_{sol} is the volume fraction of solvent, Z_{sol} is the ratio of the molar volume of solvent to the molar volume of precursor monomers, and $\vec{d}$ (q) is the change in the solubility parameter of the polymer during cross-linking. The modification takes into account the change in the number of polymer molecules with functional group conversion and allows for the construction of phase diagrams based on conversion at a constant temperature. A schematic phase diagram for CIPS is shown in Figure 1B. The phase diagram shows that a completely miscible system comprised of reactive precursors (polymer) and poragen (solvent) in the uncured state ($q = 0$) can enter either the metastable or the spinodal decomposition region to form a phase separated structure depending on the concentration of polymer, rate of curing, and extent of curing. This transition can be considered as chemical quenching.

While thermodynamic models based on first principles are useful for identifying systems that will undergo CIPS, they do not allow for an accurate prediction of morphology because the morphology produced with CIPS depends strongly on molecular mobility, which changes dramatically as cross-linking proceeds. For example, pore size for materials that undergo phase separation by a nucleation and growth mechanism will be a result of the competition that exists between the reduction in free energy achieved by pore formation and the ability of solvent molecules to diffuse through the developing polymer network. Due to the complexity of pore formation associated with CIPS, extensive structure–process–property relationships are needed to understand the influence of these variables on material properties.

Considering the number of variables and the importance of interactions between variables on the production of porous networks using the process of CIPS, it was believed that the application of high-throughput/combinatorial (HT/C) methods would significantly facilitate the development of porous polymer networks using CIPS. The HT/C methodology originated within the pharmaceutical industry to reduce the time and cost required for discovering new bioactive compounds.[20] Due to the success of the HT/C approach in the pharmaceutical industry, it has more recently been applied to material research and development. Examples of material research and development involving the HT/C methodology include

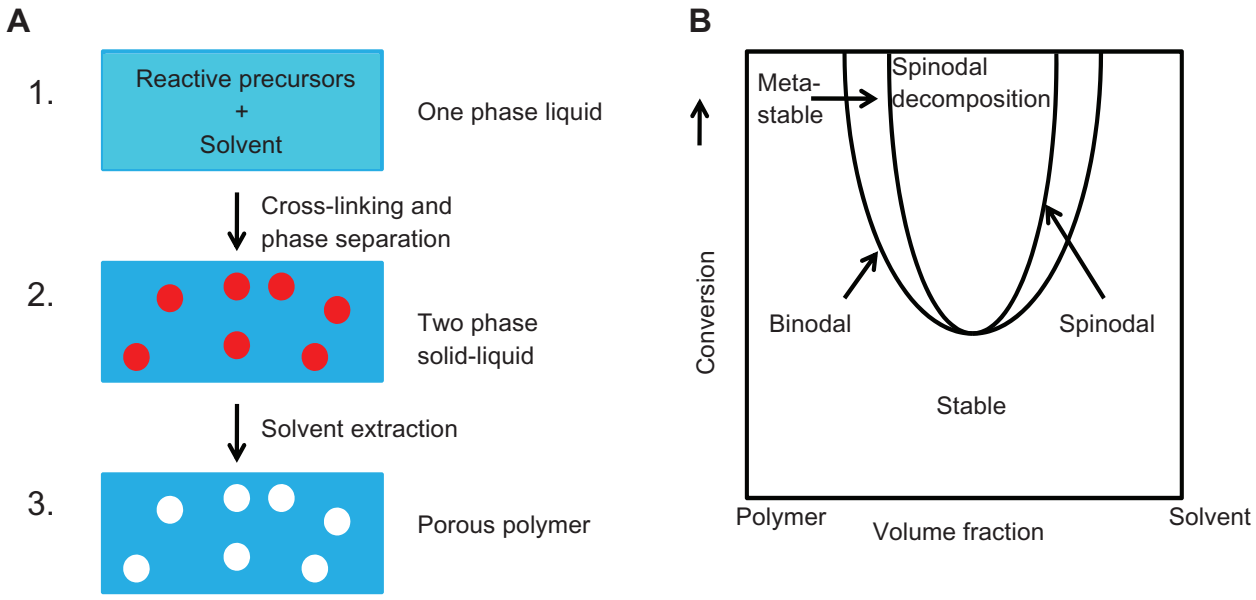

Figure 1 (**A**) An illustration of porous network structure formation using chemically induced phase separation. (**B**) Phase diagram for chemically induced phase separation.

luminescent materials,[21] surface coatings,[22,23] catalysts,[24] sensors,[25] and polymers[26,27] to name a few. In general, HT/C workflows for material development involve the use of robotics to synthesize materials in parallel, HT analytical techniques to rapidly characterize the materials and determine their critical properties of interest, and software to facilitate experimental design, control of robotic instrumentation, and data analysis. The application of HT/C methods for the generation of structure–process–property relationships for polymer materials has been shown to be very powerful.[28–31] The ability to generate and characterize relatively large numbers of materials within a relatively short period of time enables the multivariable experiments required to identify complex interactions between variables. This document describes initial efforts to construct a HT/C workflow for the generation of structure–process–property relationships for porous polymer materials produced with the process of CIPS. Results obtained for a relatively large experiment involving porous epoxy networks is described which shows that considerable information can be gained by simply monitoring changes in opacity of reactive blends as they cure. In addition, the morphology of select compositions was characterized using scanning electron microscopy (SEM).

Experimental

Materials

Table 1 describes the materials used for the experiment and Table 2 describes each of the blends prepared. All materials were used as received from the manufacturer.

Instrumentation

Liquid blends were prepared robotically using a Symyx Viscous Liquid Handling System (Symyx, Santa Clara, CA). The liquid handling robot has the capability to formulate arrays of 24 polymer blends at one time. Liquid dispensing is performed using positive displacement disposable pipette tips. The commercial formulation system was modified to allow for the use of disposable cups in conjunction with magnetic stirring.

Poragen extraction using super critical CO_2 was carried out using the device shown in Figure 2. This device consists of a 600 mL Parr™ pressure vessel (model 4765Q-T-SS; Parr Instrument Company, Moline IL) fitted with a 64-position sample holder. Liquid CO_2 is fed into the vessel in batch fashion through a dip tube in the CO_2 supply cylinder. The vessel is then heated above the critical point using a circulating water bath for stable control of the extraction temperature.

A Bhodan Balance Automator™ (model BA-100; Mettler-Toledo, Columbus, OH) was used to facilitate measurements of the weight of cured polymer discs before and after poragen extraction. Each disc was placed in an 8 mL vial. The vials were transported to and from the balance using an automated arm, and the results electronically recorded.

Samples for SEM experiments were mounted on aluminum mounts and coated with gold or platinum. SEM images were taken either with a JEOL JSM-6300scanning electron microscope or with a FEG-SEM JEOL 6700 (JEOL, Tokyo, Japan).

A DSC Q1000 (TA Instruments, New Castle, DE) equipped with an autosampler was used for measuring glass transition temperature (T_g). Samples were measured using a heat–cool–heat cycle extending from –90°C to +240°C and a heating/cooling rate of 10°C/minute.

Software

Design-Expert® (v 7.1.6; Stat.ease, Minneapolis, MN) and Symyx Library Studio® (v 7.1.3.10; Symyx Tools, Inc, Sunnyvale, CA) were used for experimental design. Epoch® (v 4.0.3.10; Symyx Tools, Inc) was used to control the Symyx Viscous Liquid Handling System (Symyx Tools, Inc).

Table 1 A description of the starting materials used for the study

Material ID	Description	Trade name	Manufacturer
Ep	Bisphenol-A-diglycidyl ether	Epon™ Resin 825	Momentive, Columbus, OH
Lxl	Amino-terminated polypropylene glycol with molecular weight 230 g/moL	Jeffamine® D-230	Huntsman, Salt Lake City, UT
Mxl	Amino-terminated polypropylene glycol with molecular weight 430 g/moL	Jeffamine® D-400	Huntsman, Salt Lake City, UT
Hxl	Amino-terminated polypropylene glycol with molecular weight 2000 g/moL	Jeffamine® D-2000	Huntsman, Salt Lake City, UT
MCHA	4,4′-Methylenebis(cyclohexylamine)	–	Aldrich, St Louis, MO
De	Decane	–	Aldrich, St Louis, MO
Dol	n-Decanol	–	Aldrich, St Louis, MO
PMA	Propylene glycol methyl ether acetate	–	Aldrich, St Louis, MO
EEP	Ethyl-3-ethoxy propionate	–	Aldrich, St Louis, MO
MAK	2-Heptanone	–	Aldrich, St Louis, MO
DBK	2,6-Dimethyl-4-heptanone	–	Aldrich, St Louis, MO

Table 2 Composition of each of the blends prepared (all weights are in grams)

Sample identifier	Wt Ep	Cross-linker	Wt cross-linker	Poragen	Wt poragen
Lxl-10De	7.00	Lxl	2.33	De	0.70
Lxl-10Dol	7.00	Lxl	2.33	Dol	0.80
Lxl-10PMA	7.00	Lxl	2.33	PMA	0.88
Lxl-10EEP	7.00	Lxl	2.33	EEP	0.91
Lxl-10MAK	7.00	Lxl	2.33	MAK	0.79
Lxl-10DBK	7.00	Lxl	2.33	DBK	0.76
Lxl-25De	7.00	Lxl	2.33	De	2.10
Lxl-25Dol	7.00	Lxl	2.33	Dol	2.39
Lxl-25PMA	7.00	Lxl	2.33	PMA	2.64
Lxl-25EEP	7.00	Lxl	2.33	EEP	2.73
Lxl-25MAK	7.00	Lxl	2.33	MAK	2.36
Lxl-25DBK	7.00	Lxl	2.33	DBK	2.32
Lxl-40De	7.00	Lxl	2.33	De	4.20
Lxl-40Dol	7.00	Lxl	2.33	Dol	4.77
Lxl-40PMA	7.00	Lxl	2.33	PMA	5.28
Lxl-40EEP	7.00	Lxl	2.33	EEP	5.47
Lxl-40MAK	7.00	Lxl	2.33	MAK	4.72
Lxl-40DBK	7.00	Lxl	2.33	DBK	4.65
Mxl-10De	7.00	Mxl	4.47	De	0.89
Mxl-10Dol	7.00	Mxl	4.47	Dol	1.01
Mxl-10PMA	7.00	Mxl	4.47	PMA	1.12
Mxl-10EEP	7.00	Mxl	4.47	EEP	1.16
Mxl-10MAK	7.00	Mxl	4.47	MAK	1.00
Mxl-10DBK	7.00	Mxl	4.47	DBK	0.98
Mxl-25De	7.00	Mxl	4.47	De	2.66
Mxl-25Dol	7.00	Mxl	4.47	Dol	3.03
Mxl-25PMA	7.00	Mxl	4.47	PMA	3.35
Mxl-25EEP	7.00	Mxl	4.47	EEP	3.47
Mxl-25MAK	7.00	Mxl	4.47	MAK	2.99
Mxl-25DBK	7.00	Mxl	4.47	DBK	2.95
Mxl-40De	7.00	Mxl	4.47	De	5.33
Mxl-40Dol	7.00	Mxl	4.47	Dol	6.05
Mxl-40PMA	7.00	Mxl	4.47	PMA	6.70
Mxl-40EEP	7.00	Mxl	4.47	EEP	6.94
Mxl-40MAK	7.00	Mxl	4.47	MAK	5.99
Mxl-40DBK	7.00	Mxl	4.47	DBK	5.90
Hxl-10De	3.50	Hxl	9.99	De	1.15
Hxl-10Dol	3.50	Hxl	9.99	Dol	1.30
Hxl-10PMA	3.50	Hxl	9.99	PMA	1.44
Hxl-10EEP	3.50	Hxl	9.99	EEP	1.49
Hxl-10MAK	3.50	Hxl	9.99	MAK	1.29
Hxl-10DBK	3.50	Hxl	9.99	DBK	1.27
Hxl-25De	3.50	Hxl	9.99	De	3.44
Hxl-25Dol	3.50	Hxl	9.99	Dol	3.91
Hxl-25PMA	3.50	Hxl	9.99	PMA	4.33
Hxl-25EEP	3.50	Hxl	9.99	EEP	4.48
Hxl-25MAK	3.50	Hxl	9.99	MAK	3.87
Hxl-25DBK	3.50	Hxl	9.99	DBK	3.81
Hxl-40De	3.50	Hxl	9.99	De	6.88
Hxl-40Dol	3.50	Hxl	9.99	Dol	7.82
Hxl-40PMA	3.50	Hxl	9.99	PMA	8.66
Hxl-40EEP	3.50	Hxl	9.99	EEP	8.96
Hxl-40MAK	3.50	Hxl	9.99	MAK	7.73
Hxl-40DBK	3.50	Hxl	9.99	DBK	7.62
MCHA-10De	7.00	MCHA	2.04	De	0.66
MCHA-10Dol	7.00	MCHA	2.04	Dol	0.75
MCHA-10PMA	7.00	MCHA	2.04	PMA	0.84
MCHA-10EEP	7.00	MCHA	2.04	EEP	0.86
MCHA-10MAK	7.00	MCHA	2.04	MAK	0.75
MCHA-10DBK	7.00	MCHA	2.04	DBK	0.74
MCHA-25De	7.00	MCHA	2.04	De	1.99
MCHA-25Dol	7.00	MCHA	2.04	Dol	2.26
MCHA-25PMA	7.00	MCHA	2.04	PMA	2.51
MCHA-25EEP	7.00	MCHA	2.04	EEP	2.59
MCHA-25MAK	7.00	MCHA	2.04	MAK	2.24
MCHA-25DBK	7.00	MCHA	2.04	DBK	2.21
MCHA-40De	7.00	MCHA	2.04	De	3.98
MCHA-40Dol	7.00	MCHA	2.04	Dol	4.52
MCHA-40PMA	7.00	MCHA	2.04	PMA	5.01
MCHA-40EEP	7.00	MCHA	2.04	EEP	5.19
MCHA-40MAK	7.00	MCHA	2.04	MAK	4.48
MCHA-40DBK	7.00	MCHA	2.04	DBK	4.41
MCHA-60Dol	3.50	MCHA	1.02	Dol	5.09

Abbreviations: DBK, 2,6-Dimethyl-4-heptanone; De, decane; Dol, n-Decanol; EEP, Ethyl-3-ethoxy propionate; Ep, bisphenol-A-diglycidyl ether; Hxl, amino-terminated polypropylene glycol with molecular weight 2000 g/moL; MAK, 2-Heptanone; MCHA, 4,4′-methylenebis(cyclohexylamine); Lxl, amino-terminated polypropylene glycol with molecular weight 230 g/moL; Mxl, amino-terminated polypropylene glycol with molecular weight 430 g/moL; PMA, propylene glycol methyl ether acetate; wt, weight.

Results and discussion

Description of the HT/C workflow

Figure 3 provides a schematic illustration of the high-throughput workflow that was developed to study the structure–process–property relationships for porous polymer materials produced with the process of CIPS. With this workflow, the experimental design was created using Design-Expert software and the design transferred into Symyx Library Studio, which was used by Epoch to control the formulation robot. Blends of the polymer network-forming precursors and poragen were prepared robotically using a Symyx Viscous Liquid Handling System.

Once the liquid blends were prepared, they were transferred to 20 mL glass vials for the curing step. Each glass vial was filled with approximately 10 mL of liquid blend and the vial capped. The capped vials were then placed in a forced air oven to cure. Once cured, the samples were allowed to cool to room temperature before extracting a cylindrical specimen from each sample using the boring device shown in Figure 4. From the cylindrical specimen, discs approximately 1.0 mm in diameter and 2.0 mm thick were prepared by slicing with a lever-action slicer (Figure 4). The weight of each disc was measured with the assistance of a Bhodan weighing robot.

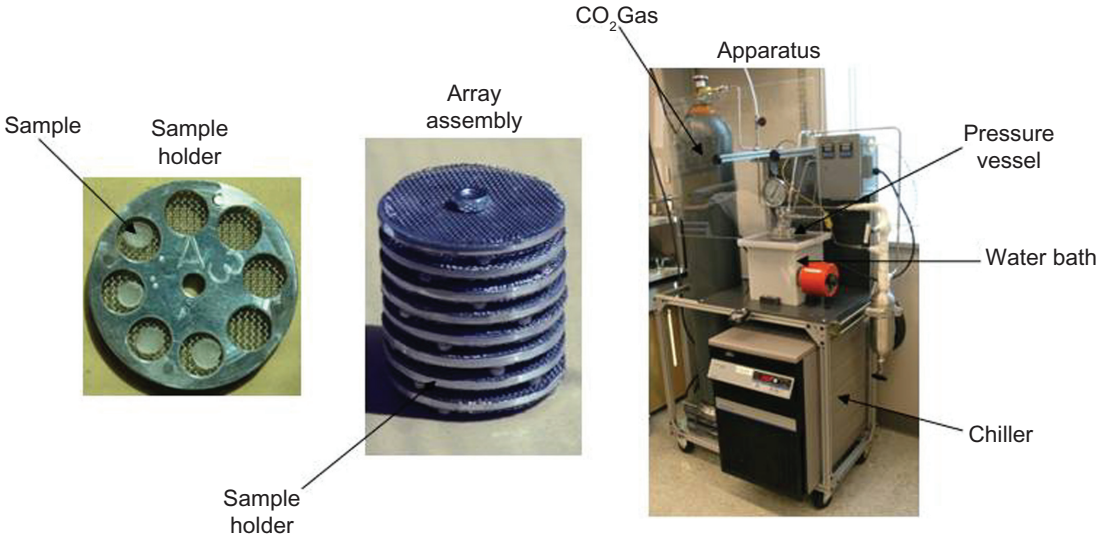

Figure 2 An image of the device used for poragen extraction of an array of 64 samples.

Once the sample discs were weighed, the poragen was extracted using super critical CO_2 and a custom-built sample holder (Figure 2) capable of holding 64 specimens. To ensure effective poragen removal, the extracted sample discs were reweighed using the weighing robot and the weight loss resulting from extraction compared with the weight of poragen used to prepare the material. SEM was used to characterize porosity and material morphology.

Porous epoxy networks produced using CIPS

An experiment was designed to investigate the effects of various compositional factors as well as cure temperature on the porosity of porous epoxy networks produced using CIPS. The epoxy-functional precursor used for the study was the diglycidyl ether of bisphenol A (Ep). In order to investigate the effect of cross-link density, a series of amino-terminated

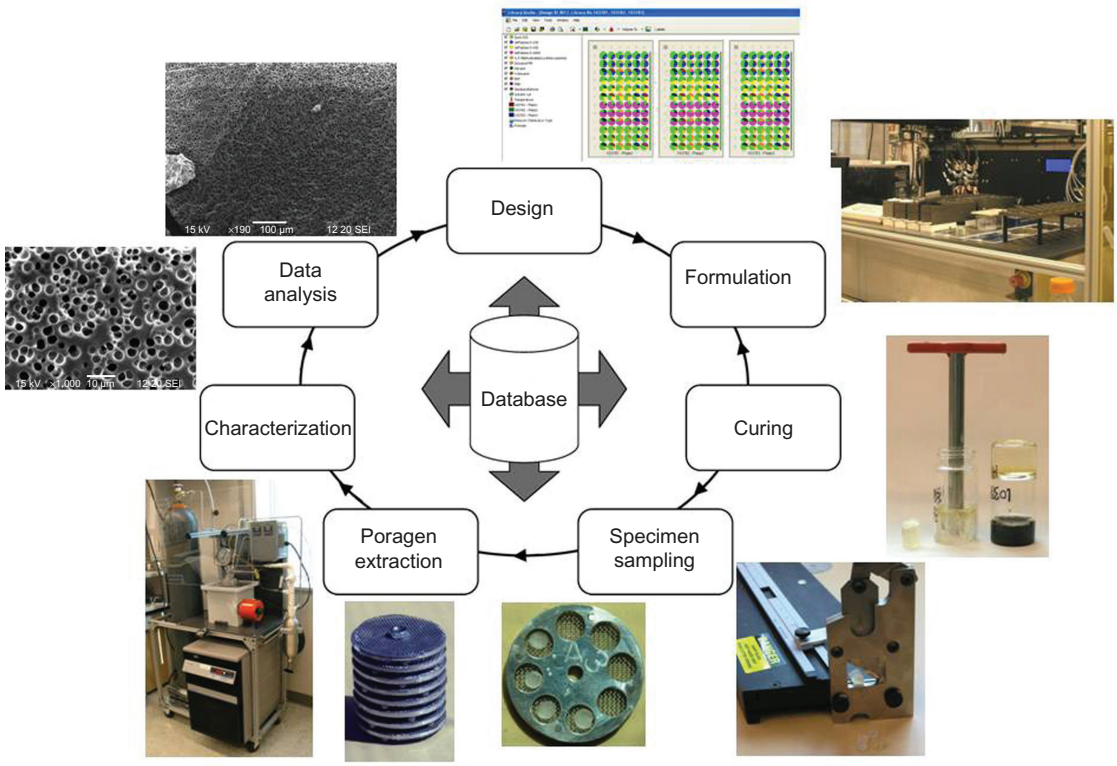

Figure 3 A schematic illustration of the high-throughput workflow that was developed.

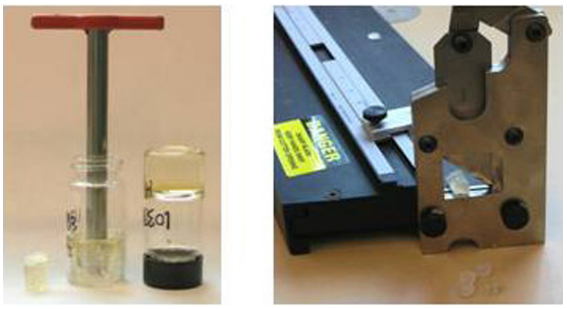

Figure 4 The boring device used to extract cylindrical specimens of cured material (left) and the device used for preparing sample discs from the cylindrical specimen (right).

polypropylene glycol oligomers of varying molecular weight was used as the cross-linker. For all samples, the molar ratio of epoxy groups to amino groups was kept constant at 2:1. In addition to the series of amino-terminated polypropylene glycol oligomers, 4,4′-methylenebis(cyclohexyl amine) (MCHA) was used as an additional cross-linker in the study.

A series of poragens possessing systematic variations in chemical structure was used for the experiment. As shown in Table 3, the molecular size of the poragens was similar, but the characteristics of their solubility parameter varied considerably. Based on thermodynamic considerations, it was expected that the use of this series of poragens would result in a range of behaviors with respect to the process of CIPS. In addition to poragen chemical composition, poragen concentration was varied at 10%, 25%, and 40% by volume.

In addition to the compositional variables described above, cure temperature was varied at 40, 80, and 120°C. Figure 5 displays a schematic illustrating the overall experimental design. A total of 216 unique compositions were used

Table 3 Solubility parameters for poragens, polymer network-forming precursors, and polymer networks

Compounds	Chemical structure	BP (°C)	Solubility parameter $(J/cm^3)^{1/2}$			
			Δ	δ_d	δ_p	δ_h
De	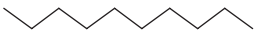	174	15.4	15.4	0.0	0.0
Dol	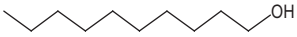	231	20.4	17.6	2.7	10.0
PMA	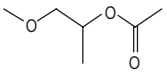	146	18.4	16.1	6.1	6.6
EEP	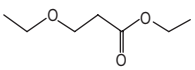	170	19.6	16.2	3.3	8.8
MAK	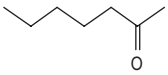	151	17.6	16.2	5.7	4.1
DBK	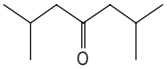	165–170	16.1	15.2	4.4	3.4
Ep	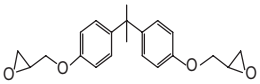	–	18.2	16.9	1.4	6.4
Lxl	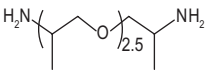	–	17.1	14.2	6.5	7.0
Mxl	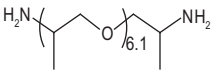	–	17.5	14.6	6.7	7.1
Hxl	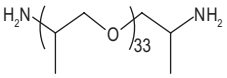	–	17.8	14.8	6.8	7.2
MCHA	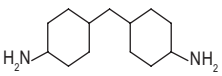	–	20.3	18.3	0.0	8.7
Ep-Lx1	Cross-linked network	–	19.9	17.1	3.7	9.5
Ep-Mx1	Cross-linked network	–	18.9	16.1	4.8	8.6
Ep-Hx1	Cross-linked network	–	18.8	15.9	6.5	7.7
EP-MCHA	Cross-linked network	–	20.4	18.9	1.4	7.5

Abbreviations: BP, boiling point; DBK, 2,6-Dimethyl-4-heptanone; De, decane; Dol, n-Decanol; EEP, Ethyl-3-ethoxy propionate; Ep, bisphenol-A-diglycidyl ether; Hxl, amino-terminated polypropylene glycol with molecular weight 2000 g/moL; MAK, 2-Heptanone; MCHA, 4,4′-methylenebis(cyclohexylamine); Lxl, amino-terminated polypropylene glycol with molecular weight 230 g/moL; Mxl, amino-terminated polypropylene glycol with molecular weight 430 g/moL; PMA, propylene glycol methyl ether acetate.

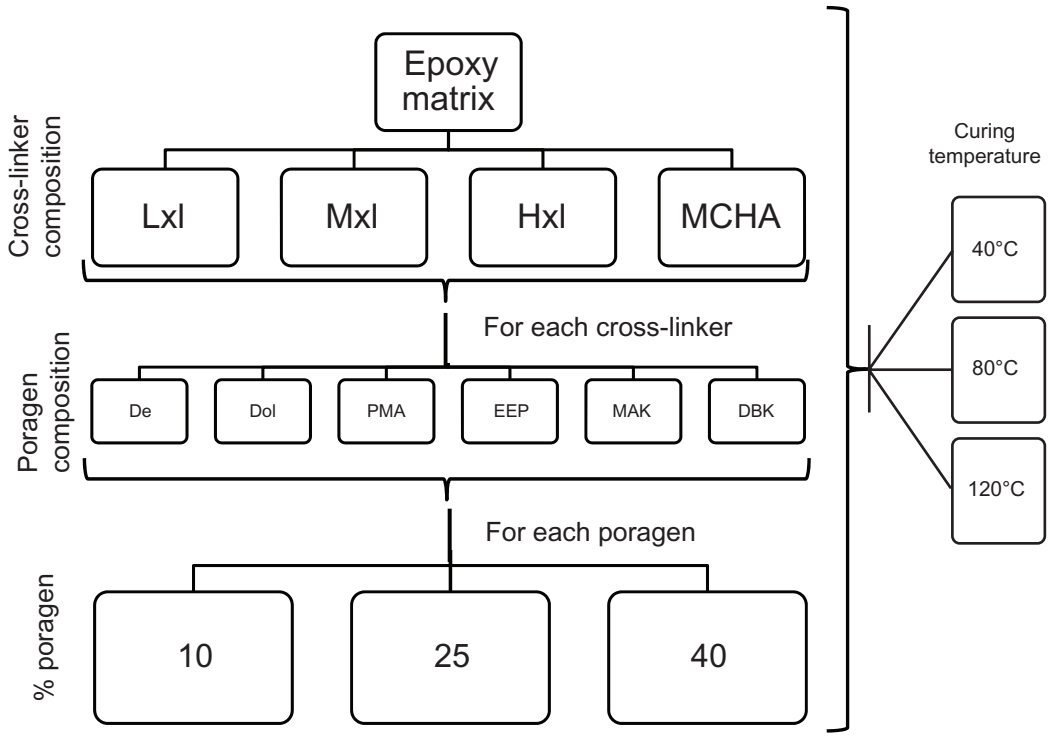

Figure 5 A schematic illustration of the experimental design used for the study. Total unique compositions = (4 cross-linkers) x (6 poragens) x (3 levels of poragen) x (3 cure temperatures) = 216.

Abbreviations: DBK, 2,6-Dimethyl-4-heptanone; De, decane; Dol, n-Decanol; EEP, Ethyl-3-ethoxy propionate; Ep, bisphenol-A-diglycidyl ether; Hxl, amino-terminated polypropylene glycol with molecular weight 2000 g/moL; MAK, 2-Heptanone; MCHA, 4,4′-methylenebis(cyclohexylamine); Lxl, amino-terminated polypropylene glycol with molecular weight 230 g/moL; Mxl, amino-terminated polypropylene glycol with molecular weight 430 g/moL; PMA, propylene glycol methyl ether acetate.

for the study. The convention used to identify the materials prepared was a-b-c-d, where "a" is the composition of the cross-linker, "b" is the volume percent of the poragen, "c" is the composition of the poragen, and "d" is the cure temperature in degrees Celsius.

Prior to producing the entire set of 216 materials containing poragen, samples of the thermoset matrix (no poragen) were prepared and characterized. All cross-linkers were miscible with Ep and cured materials were obtained at all three cure temperatures of interest (40°C, 80°C, and 120°C). As shown in Figure 6, T_gs decreased exponentially with cross-linker equivalent weight (g/mole NH_2). T_g did not vary with cure temperature, indicating that "full" cure was obtained at all three cure temperatures. In addition, from the SEM images shown in Figure 7, fracture surfaces were essentially featureless at the micron scale.

For the production of porous polymer materials using the process of CIPS, it is necessary that the uncured blend of Ep, cross-linker, and poragen be miscible prior to curing. Thus, observations of blend miscibility were made shortly after robotic preparation of the blends. As shown in Table 4, all blends based on propylene glycol methyl ether acetate (PMA), ethyl-3-ethoxy propionate (EEP), 2-Heptanone (MAK), and 2,6-Dimethyl-4-heptanone (DBK) were fully miscible at room temperature while limited miscibility was observed for blends based on decane (De) and n-Decanol (Dol). For blends based on De, only two materials were miscible at room temperature, namely, amino-terminated

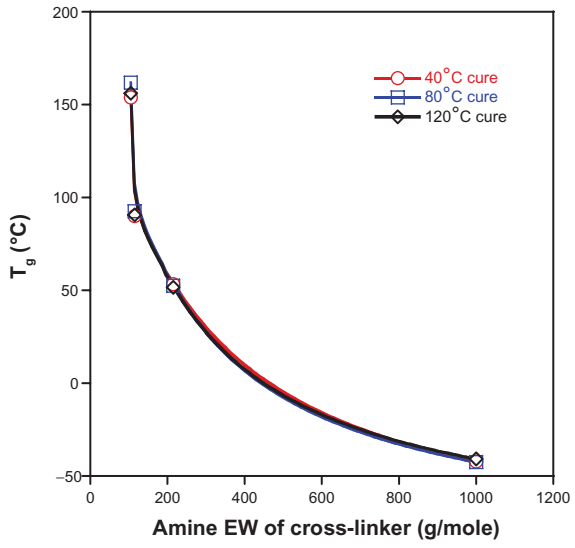

Figure 6 T_g as a function of cross-linker equivalent weight (EW; g/mole NH_2) for the cured polymer networks (no poragen).

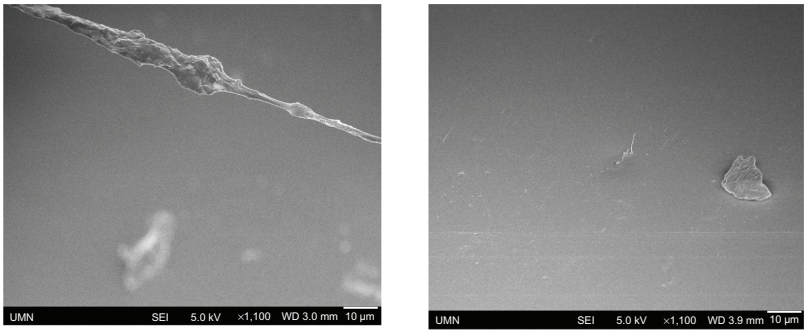

Ep-Hx1 Ep-MCHA

Figure 7 Scanning electron microscopy images of fracture surfaces obtained from cured polymer networks (no poragen).
Abbreviations: Ep, bisphenol-A-diglycidyl ether; Hxl, amino-terminated polypropylene glycol with molecular weight 2000 g/moL; MCHA, 4,4′-methylenebis(cyclohexylamine).

polypropylene glycol with molecular weight 430 g/moL (Mxl)-10De and amino-terminated polypropylene glycol with molecular weight 2000 g/moL (Hxl)-10De. For blends based on Dol, those containing Dol concentrations of 40% were immiscible while those containing Dol concentrations of 25% and 10% were miscible at room temperature. To explain the variations in blend miscibility observed, the solubility parameters for Ep and the various cross-linkers were calculated using the group-contribution method.[32] As shown in Table 3, the solubility parameter for Ep and the amino-terminated polypropylene glycol cross-linkers was 18.2 and 17.1–17.8 $(J/cm^3)^{½}$, respectively. A comparison of these solubility parameters with those of the poragens showed that the greatest difference in solubility parameter was observed for De and Dol, which was consistent with the miscibility results observed.

Table 4 Results of observations made at room temperature regarding blend miscibility

Matrix (cross-linker)	v% Poragen	Poragen					
		De	Dol	PMA	EEP	MAK	DBK
Lxl	10	–	+	+	+	+	+
	25	–	+	+	+	+	+
	40	–	–	+	+	+	+
Mxl	10	+	+	+	+	+	+
	25	–	+	+	+	+	+
	40	–	–	+	+	+	+
Hxl	10	+	+	+	+	+	+
	25	–	+	+	+	+	+
	40	–	–	+	+	+	+
MCHA	10	–	+	+	+	+	+
	25	–	+	+	+	+	+
	40	–	–	+	+	+	+

Note: "+" indicates the formation of a miscible blend while "–" indicates the formation of a two-phase blend.
Abbreviations: DBK, 2,6-Dimethyl-4-heptanone; De, decane; Dol, n-Decanol; EEP, Ethyl-3-ethoxy propionate; Ep, bisphenol-A-diglycidyl ether; Hxl, amino-terminated polypropylene glycol with molecular weight 2000 g/moL; MAK, 2-Heptanone; MCHA, 4,4′-methylenebis(cyclohexylamine); Lxl, amino-terminated polypropylene glycol with molecular weight 230 g/moL; Mxl, amino-terminated polypropylene glycol with molecular weight 430 g/moL; PMA, propylene glycol methyl ether acetate.

Due to differences in the cure rate resulting from differences in the reactive group concentration, the time required to cure the blends into solid materials varied substantially. For example, at the highest cure temperature (120°C), blends based on the lowest poragen concentration and lowest molecular weight cross-linker cured to a solid material in less than 72 hours, while blends cured at the lowest cure temperature (40°C) and based on the highest poragen concentration and highest molecular weight cross-linker required approximately 21 days to cure to a solid material. Due to these variations in cure rate, observations were periodically made to ensure that all blends had sufficiently cured before removing them from the oven.

Once cured, observations were made with regard to the visual characteristics of the materials. As shown in Figure 8, three basic material characteristics were visually observed for the blends. The production of transparent, homogeneous blends (Figure 8A) indicated complete miscibility or nanoscale phase separation while the production of a uniformly opaque (Figure 8B) or a two layer material (Figure 8C) indicated immiscibility. As shown in Table 5, 79% of the materials were transparent (Figure 8A), indicating homogeneity at the macroscopic level; 16% formed two separate layers in which the poragen separated from the cured polymer to produce a liquid layer above the cured polymer (Figure 8C); and 5% formed opaque materials in which the poragen existed as large domains within the cross-linked polymer (Figure 8B). As expected, the occurrence of macroscopic phase separation was strongly related to the composition of the poragen. All of the materials based on MAK or PMA were transparent, while macroscopic phase separation occurred for 72% of the materials based on De. Since the enthalpy of mixing is related to the difference in the solubility parameter between a solvent and polymer, the number fraction of macroscopically phase-separated materials observed

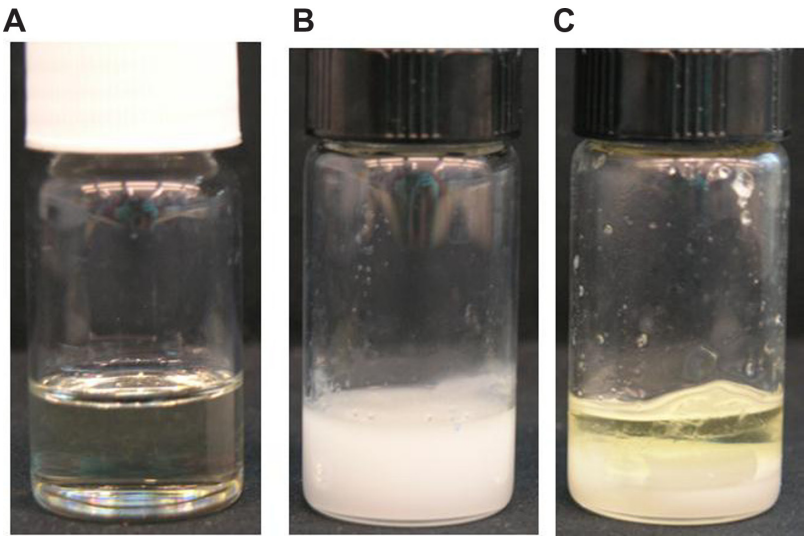

Figure 8 Images illustrating the various types of phase behavior exhibited by cured blends. (**A**) Transparent, homogeneous blend indicating complete miscibility or nanoscale phase separation; (**B**) uniformly opaque blend indicating microscale phase separation; and (**C**) blend displaying two layers that indicate gross phase separation of the poragen from the cross-linked polymer.

for a given poragen was plotted as a function of the solubility parameter of the poragen. As shown in Figure 9, the plot exhibits a minimum at a solubility parameter of about 18.5 $(J/cm^3)^{½}$. For comparison, the solubility parameter of the four different cross-linked matrices was calculated using the group contribution method.[32] As shown in Table 3, the solubility parameters for the four different cross-linked networks were 20.4, 19.9, 18.9, and 18.8 $(J/cm^3)^{½}$ for Ep-MCHA, Ep-amino-terminated polypropylene glycol with molecular weight 230 g/moL (Lxl), Ep-Mxl, and Ep-Hxl, respectively. Considering the solubility parameters calculated for the cross-linked networks, it is not surprising that the poragens possessing a solubility parameter close to 18.5 $(J/cm^3)^{½}$ gave the lowest occurrence of micron-scale phase separation.

A comparison of the phase behavior exhibited before (Table 4) and after (Table 5) curing indicated that curing did not induce macroscopic phase separation for any of the materials based on PMA [$\delta = 18.4$ $(J/cm^3)^{½}$] or MAK [$\delta = 17.6$ $(J/cm^3)^{½}$]; however, curing did induce macroscopic phase separation for blends based on DBK [$\delta = 16.1$ $(J/cm^3)^{½}$] and EEP [$\delta = 19.6$ $(J/cm^3)^{½}$]. Examination of the data displayed in Tables 4 and 5 shows that all of the materials that underwent macroscopic phase separation as a result of curing were based on the high level (40%) of poragen. The data also indicate that some uncured blends based on De and Dol that were immiscible at room temperature formed transparent materials when cured. This result suggests that, when heated to the curing temperature, the liquid blend transformed from a two-phase material to a miscible blend prior to undergoing cross-linking and CIPS did not occur. The transformation of a two-phase liquid blend to a miscible blend upon heating is consistent with the upper critical solution temperature behavior expected for the liquid blends.[15]

Monolithic discs of the samples were extracted with supercritical CO_2 and the extraction process monitored by periodically weighing the discs using a robotic weighing instrument. Extraction time was adjusted based on results obtained from sample weighing to ensure full extraction of the poragen. Since SEM, the method needed to characterize sample morphology, is relatively time and resource intensive, subsets of the 216 samples were selected for extraction

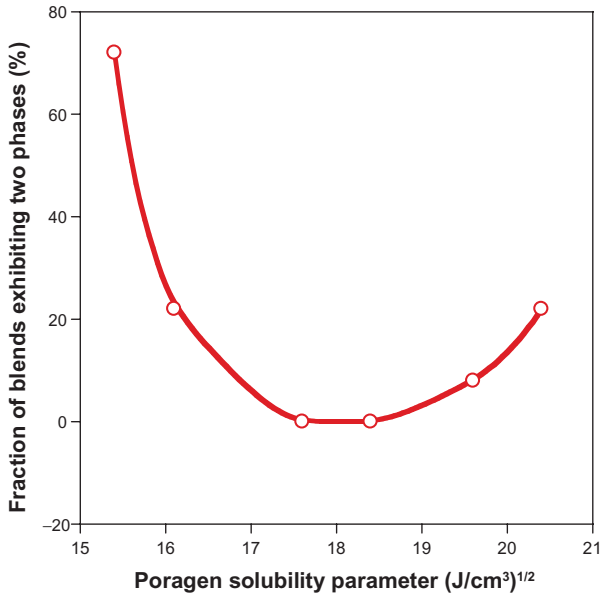

Figure 9 Phase behavior of cured blends as a function of poragen solubility parameter.

Table 5 Results of visual observations made regarding the phase behavior of the cured materials

Matrix (cross-linker)	% Poragen	Poragen																
		De			Dol			PMA			EEP			MAK			DBK		
		Cure (°C)			Cure (°C)			Cure (°C)			Cure (°C)			Cure (°C)			Cure (°C)		
		40	80	120	40	80	120	40	80	120	40	80	120	40	80	120	40	80	120
Lxl	10	O	O	T	T	T	T	T	T	T	T	T	T	T	T	T	T	T	T
	25	2L	2L	2L	T	T	T	T	T	T	T	T	T	T	T	T	T	T	T
	40	2L	2L	2L	2L	2L	O	T	T	T	T	T	2L	T	T	T	O	2L	2L
Mxl	10	O	T	T	T	T	T	T	T	T	T	T	T	T	T	T	T	T	T
	25	2L	2L	2L	T	T	T	T	T	T	T	T	T	T	T	T	T	T	T
	40	2L	2L	2L	2L	T	2L	T	T	T	T	T	T	T	T	T	T	T	2L
Hxl	10	T	T	T	T	T	T	T	T	T	T	T	T	T	T	T	T	T	T
	25	T	T	T	T	T	T	T	T	T	T	T	T	T	T	T	T	T	T
	40	2L	2L	2L	T	T	T	T	T	T	T	T	T	T	T	T	T	T	T
MCHA	10	O	T	2L	T	T	T	T	T	T	T	T	T	T	T	T	T	T	T
	25	2L	2L	2L	T	T	T	T	T	T	T	T	T	T	T	T	O	T	T
	40	2L	2L	2L	O	2L	2L	T	T	T	O	T	2L	T	T	T	O	O	2L

Note: "T" indicates the observation shown in Figure 8A, "O" indicates the observation shown in Figure 8B, and "2L" indicates the observation shown in Figure 8C.
Abbreviations: DBK, 2,6-Dimethyl-4-heptanone; De, decane; Dol, n-Decanol; EEP, Ethyl-3-ethoxy propionate; Ep, bisphenol-A-diglycidyl ether; Hxl, amino-terminated polypropylene glycol with molecular weight 2000 g/moL; MAK, 2-Heptanone; MCHA, 4,4′-methylenebis(cyclohexylamine); Lxl, amino-terminated polypropylene glycol with molecular weight 230 g/moL; Mxl, amino-terminated polypropylene glycol with molecular weight 430 g/moL; PMA, propylene glycol methyl ether acetate.

and porosity characterization. The initial material subset characterized consisted of 24 samples based on a single cross-linker (Hxl), all six poragens, two poragen concentrations (10 and 40 vol%), and two temperatures (40°C and 120°C). Figure 10 displays representative SEM images of fracture surfaces for each of the 24 samples. The images displayed in Figure 10 show three basic morphologies. (1) For many samples, such as Hxl-10PMA-120C, Hxl-40PMA-40C, and Hxl-40EEP-40C, smooth, featureless fracture surfaces equivalent to those observed for the control samples (no poragen)

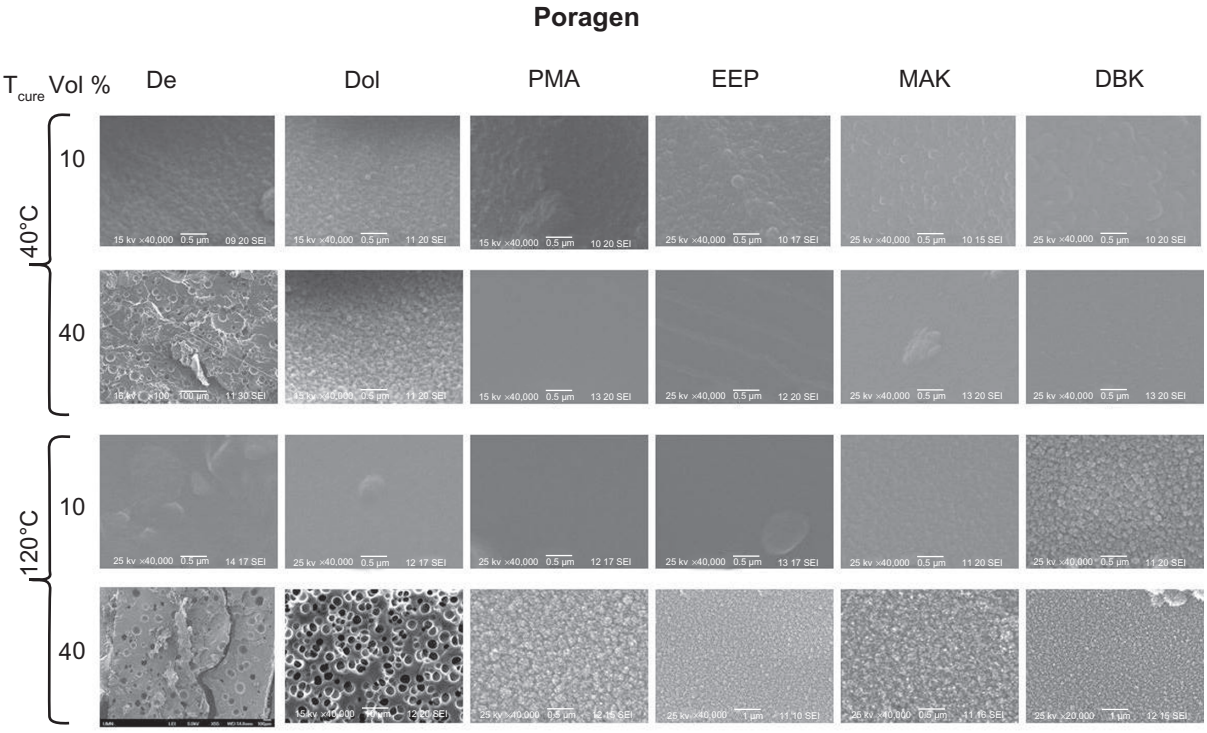

Figure 10 Representative images of fracture surfaces for 24 different samples. Sample set provides illustrations of variations in poragen composition, poragen concentration (10 and 40 vol %), and cure temperature (40°C and 120°C).
Abbreviations: DBK, 2,6-Dimethyl-4-heptanone; De, decane; Dol, n-Decanol; EEP, Ethyl-3-ethoxy propionate; MAK, 2-Heptanone; PMA, propylene glycol methyl ether acetate.

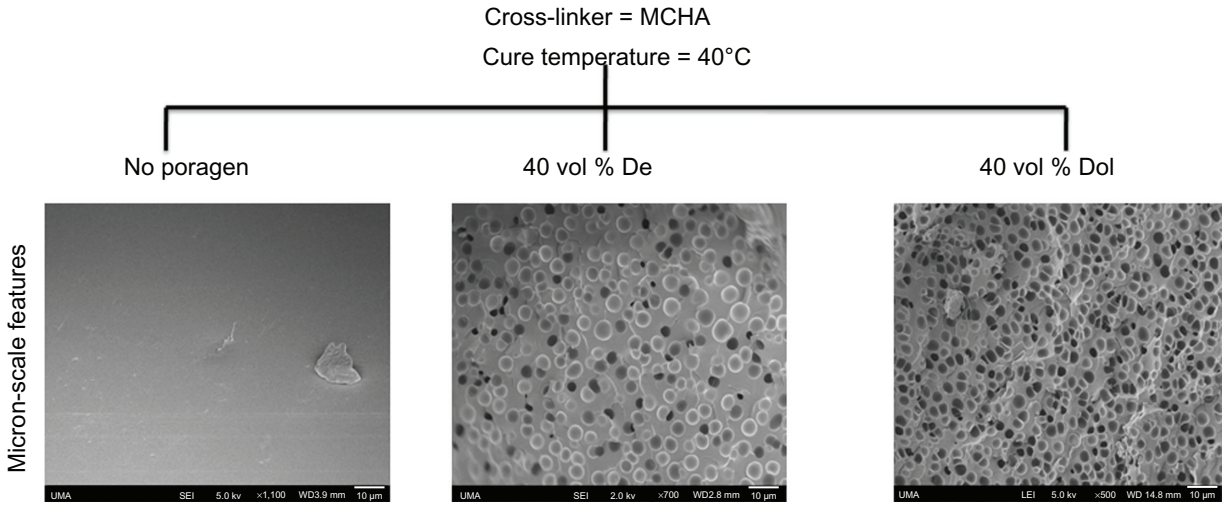

Figure 11 Scanning electron microscopy images of fracture surfaces of materials based on MCHA as the cross-linker and cured at 40°C.
Abbreviations: De, decane; Dol, n-Decanol; MCHA, 4,4′-methylenebis(cyclohexylamine).

were obtained. This morphology indicates that the material remained a stable, one-phase material over the course of cross-linking. (2) Samples Hxl-40Dol-120C, Hxl-40De-40C, and Hxl-40De-120C exhibited spherical pores consistent with CIPS occurring by a nucleation and growth mechanism. (3) The final general morphology that was observed for samples such as Hxl-40PMA-120C and Hxl-40MAK-120C consisted of a rough fracture surface in which discrete pores were not observed. This morphology may be the result of quenching phase separation at the early stage of the phase-separation process by the increase in viscosity and reduction in molecular mobility associated with the process of cross-linking. In general, the results shown in Figure 10 indicate that increasing poragen concentration and increasing cure temperature increase the tendency for the formation of a two-phase morphology; however, micron-scale pores were only observed for materials based on the two poragens that showed the lowest miscibility with the reactive precursors, namely, De and Dol. Assuming upper critical solution temperature behavior for the blend of the poragen and uncured polymer (polymer that has not yet gelled), the observation that increasing temperature promoted phase separation indicates that the increase in polymer molecular weight resulting from cross-linking reactions has a bigger effect on the thermodynamics of mixing than temperature. Figure 11 shows micron-scale pores were also observed when De and Dol were used as poragens for materials based on MCHA as the cross-linker.

Conclusion

A HT/C method was developed to study porous polymer materials produced by CIPS. Using this method, a total of 216 unique materials based on an epoxy-amine curing system were prepared. The results obtained allowed for the identification of the appropriate poragens and process conditions required to obtain porosity. In general, the use of the two poragens that exhibited limited miscibility with the polymer network precursors (De and Dol) and relatively high levels of poragen produced micron-scale porosity. A subset of materials was characterized with regard to material morphology by SEM. The pores produced from De and Dol as poragens were discrete and spherical in nature.

Acknowledgments

The authors would like to thank Sandia National Laboratories, under grant 825031, and the MRSEC program of the National Science Foundation, under award number DMR-0819885, for financial support. In addition, the authors thank Scott Payne from the USDA Microscopy Lab at North Dakota State University and Dr Bob Hafner from the University of Minnesota for microscopy.

Disclosure

The authors report no conflicts of interest in this work.

References

1. Christenson EM, Soofi W, Holm JL, Cameron NR, Mikos AG. Biodegradable fumarate-based PolyHIPEs as tissue engineering scaffolds. *Biomacromolecules*. 2007;8(12):3806–3814.
2. Vandezande P, Gevers LE, Vermant J, Martens JA, Jacobs PA, Vankelecom IF. Solidification of emulsified polymer solutions via phase inversion (SEPPI): a generic way to prepare polymers with controlled porosity. *Chem Mater*. 2008;20(10):3457–3465.
3. Eeltink S, Svec F. Recent advances in the control of morphology and surface chemistry of porous polymer-based monolithic stationary phases and their application in CEC. *Electrophoresis*. 2007;28(1–2):137–147.

4. Li TD, Gan LM, Chew CH, Teo WK, Gan LH. Preparation of ultrafiltration membranes by direct microemulsion polymerization using polymerizable surfactants. *Langmuir*. 1996;12(24):5863–5868.
5. Lushcheikin GA. New polymer-containing piezoelectric materials. *Phys Solid State*. 2006;48(6):1023–1025.
6. Vamvakaki V, Chaniotakis NA. Immobilization of enzymes into nanocavities for the improvement of biosensor stability. *Biosens Bioelectron*. 2007;22(11):2650–2655.
7. Adhikari B, Majumdar S. Polymers in sensor applications. *Prog Polym Sci*. 2004;29:699–766.
8. Germain J, Hradil J, Frechet JM, Svec F. High surface area nanoporous polymers for reversible hydrogen storage. *Chem Mater*. 2006;18:4430–4435.
9. Germain J, Svec F, Frechet JM. Preparation of size-selective nanoporous polymer networks of aromatic rings: potential adsorbents for hydrogen storage. *Chem Mater*. 2008;20:7069–7076.
10. Zhao H, Jiang C, He X, Ren J, Wan C. Preparation of micro-porous membrane electrodes and their application in preparing anodes of rechargeable lithium batteries. *J Mem Sci*. 2008;310(1–2):1–6.
11. Jin Yoon J, Ho Song S, Sung Lee D, Park TG. Immobilization of cell adhesive RGD peptide onto the surface of highly porous biodegradable polymer scaffolds fabricated by a gas foaming/salt leaching method. *Biomaterials*. 2004;25(25):5613–5620.
12. Cameron NR. High internal phase emulsion templating as a route to well-defined porous polymers. *Polymer*. 2005;46(5):1439–1449.
13. Zhang H, Cooper AI. Synthesis and applications of emulsion-templated porous materials. *Soft Matter*. 2005;1:107–113.
14. Song SW, Torkelson JM. Coarsening effects on microstructure formation in isopycnic polymer solutions and membranes produced via thermally induced phase separation. *Macromolecules*. 1994;27(22):6389–6397.
15. Kiefer J, Hedrick JL, Hilborn JG. Macroporous thermosets by chemically induced phase separation. *Adv Polym Sci*. 1999;147:161–247.
16. Hillmyer MA. Nanoporous materials from block copolymer precursors. *Adv Polym Sci*. 2005;190:137–181.
17. Wulff G. Enzyme-like catalysis by molecularly imprinted polymers. *Chem Rev*. 2002;102(1):1–27.
18. Kiefer J, Hilborn JG, Manson JA, Leterrier Y. Macroporous epoxy networks via chemically induced phase separation. *Macromolecules*. 1996;29(11):4158–4160.
19. Klein RJ, Celina MC, Lenhart JL. Porous epoxies by reaction induced phase separation of removable alcohols: control of spheroidal pore size by mass fraction, cure temperature, and reaction rate. *J Appl Poly Sci*. 2010;117(6):3300–3307.
20. Martin EJ, Critchlow RE. Beyond mere diversity: tailoring combinatorial libraries for drug discovery. *J Comb Chem*. 1999;1(1):32–45.
21. Chen L, Chu CI, Chen KJ, Chen PY, Hu SF, Liu RS. An intelligent approach to the discovery of luminescent materials using a combinatorial approach combined with Taguchi methodology. *Luminescence*. 2011;26(4):229–238.
22. Chisholm B, Potyrailo R, Cawse J, et al. The development of combinatorial chemistry methods for coating development: I. Overview of the experimental factory. *Prog Org Coat*. 2002;45(2–3):313–321.
23. Webster DC, Bennett J, Kuebler S, Kossuth MB, Jonasdottir S. High throughput workflow for the development of coatings. *JCT Coatings Tech*. 2004;1:34–39.
24. Kirsten G, Maier WF. Strategies for the discovery of new catalysts with combinatorial chemistry. *Appl Surf Sci*. 2004;223(1–3):87–101.
25. Basabe-Desmonts L, Beld J, Zimmerman RS, et al. A simple approach to sensor discovery and fabrication on self-assembled monolayers on glass. *J Am Chem Soc*. 2004;126(23):7293–7299.
26. Cawse JN. Experimental strategies for combinatorial and high-throughput materials development. *Acc Chem Res*. 2001;34(3):213–221.
27. Tourniaire G, Collins J, Campbell S, et al. Polymer microarrays for cellular adhesion. *Chem Commun*. 2006;20:2118–2120.
28. Majumdar P, Lee E, Patel N, et al. Combinatorial materials research applied to the development of new surface coatings IX: an investigation of novel antifouling/fouling-release coatings containing quaternary ammonium salt groups. *Biofouling*. 2008;24(3):185–200.
29. Majumdar P, Stafslien S, Daniels J, Webster DC. High throughput combinatorial characterization of thermosetting siloxane-urethane coatings having spontaneously formed microtopographical surfaces. *J Coat Technol Res*. 2007;4(2):131–138.
30. Majumdar P, Lee E, Gubbins N, et al. Combinatorial materials research applied to the development of new surface coatings XIII: an investigation of polysiloxane antimicrobial coatings containing tethered quaternary ammonium salt groups. *J Comb Chem*. 2009;11(6):1115–1127.
31. Ekin A, Webster DC, Daniels JW, et al. Synthesis, formulation, and characterization of siloxane–polyurethane coatings for underwater marine applications using combinatorial high-throughput experimentation. *J Coat Technol Res*. 2007;4(4):435–451.
32. Brandrup J, Immergut EH, Grulke EA. *Polymer Handbook*. 4th ed. New York, NY: Wiley; 1998:2.